remote sensing

MDPI

Article

Quantifying the Impact of Crude Oil Spills on the Mangrove Ecosystem in the Niger Delta Using AI and Earth Observation

Jemima O'Farrell [1,2], Dualta O'Fionnagáin [1,2], Abosede Omowumi Babatunde [3], Micheal Geever [1,2], Patricia Codyre [1,2], Pearse C. Murphy [1,2], Charles Spillane [2,4] and Aaron Golden [1,2,*]

1 School of Natural Sciences, College of Science and Engineering, University of Galway, Galway H91 TK33, Ireland; jemima.ofarrell@universityofgalway.ie (J.O.); dualta.ofionnagain@universityofgalway.ie (D.O.); michael.geever@universityofgalway.ie (M.G.); patricia.codyre@universityofgalway.ie (P.C.); pearse.murphy@universityofgalway.ie (P.C.M.)
2 Ryan Institute, University of Galway, Galway H91 TK33, Ireland; charles.spillane@universityofgalway.ie
3 Centre for Peace and Strategic Studies, University of Ilorin, Kwara 240102, Nigeria; babatunde.ar@unilorin.edu.ng
4 School of Biological and Chemical Sciences, College of Science and Engineering, University of Galway, Galway H91 TK33, Ireland
* Correspondence: aaron.golden@universityofgalway.ie

Abstract: The extraction, processing and transport of crude oil in the Niger Delta region of Nigeria has long been associated with collateral environmental damage to the largest mangrove ecosystem in Africa. Oil pollution is impacting not only one of the planet's most ecologically diverse regions but also the health, livelihoods, and social cohesion of the Delta region inhabitants. Quantifying and directly associating localised oil pollution events to specific petrochemical infrastructure is complicated by the difficulty of monitoring such vast and complex terrain, with documented concerns regarding the thoroughness and impartiality of reported oil pollution events. Earth Observation (EO) offers a means to deliver such a monitoring and assessment capability using Normalised Difference Vegetation Index (NDVI) measurements as a proxy for mangrove biomass health. However, the utility of EO can be impacted by persistent cloud cover in such regions. To overcome such challenges here, we present a workflow that leverages EO-derived high-resolution (10 m) synthetic aperture radar data from the Sentinel-1 satellite constellation combined with machine learning to conduct observations of the spatial land cover changes associated with oil pollution-induced mangrove mortality proximal to pipeline networks in a 9000 km^2 region of Rivers State located near Port Harcourt. Our analysis identified significant deforestation from 2016–2024, with an estimated mangrove mortality rate of 5644 hectares/year. Using our empirically derived Pipeline Impact Indicator (PII), we mapped the oil pipeline network to 1 km resolution, highlighting specific pipeline locations in need of immediate intervention and restoration, and identified several new pipeline sites showing evidence of significant oil spill damage that have yet to be formally reported. Our findings emphasise the critical need for the continuous and comprehensive monitoring of oil extractive regions using satellite remote sensing to support decision-making and policies to mitigate environmental and societal damage from pipeline oil spills, particularly in ecologically vulnerable regions such as the Niger Delta.

Keywords: remote sensing; Earth observation; machine learning; synthetic aperture radar; landcover; pollution; Niger Delta; mangroves

check for updates

Academic Editor: Dehua Mao

Received: 2 December 2024
Revised: 10 January 2025
Accepted: 20 January 2025
Published: 22 January 2025

Citation: O'Farrell, J.; O'Fionnagáin, D; Babatunde, A.O.; Geever, M.; Codyre, P.; Murphy, P.C.; Spillane, C.; Golden, A. Quantifying the Impact of Crude Oil Spills on the Mangrove Ecosystem in the Niger Delta Using AI and Earth Observation. *Remote Sens.* **2025**, *1*, 358. https://doi.org/10.3390/rs17030358

Copyright: © 2025 by the authors. Licensee MDPI, Basel, Switzerland. This article is an open access article distributed under the terms and conditions of the Creative Commons Attribution (CC BY) license (https://creativecommons.org/licenses/by/4.0/).

1. Introduction

The Niger Delta mangrove forests, spanning nine coastal states of Nigeria, are of major ecological significance as biodiversity hotspots. These forests harbour extensive biodiversity, including many endangered species [1]. Additionally, they are a vital resource for climate change mitigation as they sequester substantial quantities of atmospheric carbon dioxide [2]. The Niger Delta contains Africa's largest mangrove swamp and the world's third-largest wetland [3,4]. Beyond their ecological value, these mangrove forests play a crucial role in the lives of the diverse communities of the Niger Delta. For instance, these coastal forests serve as nurseries for young fish, supporting a vital food resource, yet the unmet demand for fish in Nigeria continues to rise [5]. With 70% of the population of the Niger Delta residing in rural areas, most depend on agricultural and piscatorial subsistence practices for their livelihoods and food security, as well as their cultural identity and well-being [6].

The Niger Delta region, with a 70-year history of oil extraction, hosts the second largest petroleum reserve on the African continent, with some estimates of up to 40.5 billion barrels of crude oil located within the lower Delta [7]. Nigeria's economy is heavily reliant on oil production, and associated oil exploration activities are attributed to over 90% of Nigeria's national foreign exchange [8]. However, oil operations in the Niger Delta have also been associated with numerous oil spillage and other pollution incidents resulting in well-documented environmental, social, and cultural impacts, including negative effects on fishing and farming sectors, adverse human health impacts, and disruption of the social and cultural fabric of affected communities [3,4,9–11].

Despite the persistent environmental consequences of oil pollution, policies and policy implementation processes have yet to show effective mitigation of oil pollution in the Niger Delta. A number of independent assessments have identified a range of complex issues impeding mitigation progress, including a lack of effective government interventions, violent contestations over compensation, equipment failures, and self-regulatory maintenance oversight of oil facilities by petroleum companies. Additionally, theft, artisanal oil refining, and oil bunkering, activities driven by economic pressures, contribute to the many obstacles to the oil pollution clean-up and environmental restoration efforts planned for the Niger Delta [4,10,12,13].

Since 2006, the Nigerian government's National Oil Spill Detection and Response Agency (NOSDRA) have reported over 130,000,000 litres of crude oil spillages in the Niger Delta [14]. A range of studies have attempted to quantify the extent of the oil spills, but the estimated total amount remains inherently imprecise due to under-reporting, incomplete data and limited monitoring and oversight [15]. Additionally, under-investment in NOSDRA's abilities to fully implement its statutory mandate [16], has resulted in reports of the petrochemical industry spearheading spillage investigations [17], with associated concerns about conflicts of interest.

The United Nations Environment Programme (UNEP) 2011 report provided one of the first independent comprehensive multi-disciplinary reports on the environmental and human impacts of oil pollution in the region [10]. It highlighted the adverse effects on vegetative and aquatic systems, air quality, and the additional strain on public health and socio-economic stability in the Niger Delta. More recent research indicates that as of 2016, over one million individuals resided within the pollution-affected region surrounding Ogoniland [18], where pollutants bio-accumulate along the food chain, with both the air and drinking water being highly contaminated [19]. Whilst this report has been significant as an advocacy tool for affected communities and a benchmark resource to raise awareness among policymakers, such reports have limitations, including restricted spatial coverage, sampling bias due to site accessibility, and narrow temporal scope.

Efforts to more precisely quantify the full extent of the effects of petroleum contamination have been hindered by the cost associated with comprehensive field-based surveys. Traditional field surveys are costly, time-consuming, and largely unsuitable for continuous monitoring, which greatly restricts understanding of the full-scale impact of oil spills. Leveraging remote sensing from low Earth orbit satellites offers a promising avenue to overcome these limitations and enhance assessment, by simultaneously identifying and characterising visible changes in biomass, infrastructure, and local natural resources coincident with reported oil spillage locations, particularly given the spatiotemporal coverage available. This is of particular relevance to the Niger Delta region, where the clearest proxy for localised ecosystem health on the ground is the status of its mangrove forests.

Remotely sensing any given location's biomass status using satellites is traditionally enabled by the use of optically derived vegetative health indices, which capture a range of biophysical parameters. Prominent examples include the Normalized Difference Vegetation Index (NDVI) and the Leaf Area Index (LAI), both of which have seen increased accessibility in recent years, owing to the emergence of extensive catalogues featuring analysis-ready Earth Observation (EO) data products [20]. However, it is crucial to acknowledge the inherent limitations of passive optical sensors, namely their vulnerability to cloud cover and illumination variations, which are persistent issues in tropical regions such as the Niger Delta. For Sentinel-2 optical data over our region of interest between 2016 and 2023, there were only a total of 369 available scenes where the average cloud cover was 72% and only 22 scenes had a cloudy pixel percentage of less than 20%. Having access to such a limited number of adequate-quality scenes underscores the issue of sampling different stages of the phenology year-on-year. This challenge renders monitoring via passive optical sensors unreliable with sizable temporal gaps between measurements.

The advent of open-access active sensors, such as Sentinel-1, presents an alternative solution. In particular, synthetic aperture radar (SAR) offers insights into target structure via backscatter intensity and polarisation, where the timeliness and reliability of the observations are facilitated by its cloud-penetrating, all-weather, and illumination-independent sensing capabilities [21]. This study utilises the timeliness and reliability of Sentinel-1, in conjunction with machine learning classification techniques, to establish a novel and powerful workflow that can identify zones within the mangrove forests of the Niger Delta that are highly impacted by oil spillage events. We specifically focus on highly polluted areas to assess and quantify the extent of mangrove damage over time in proximity to known pipeline infrastructures and spillages.

Study Region

Our region of interest within the Niger Delta covers just over 5200 km^2 of land and about 3500 km^2 of permanent water bodies (Figure 1), encompassing the coastal portion of Rivers State in Nigeria, with the capital Port Harcourt located to the North, and the urban settlements of Bonny Island to the Southeast and Bille situated slightly East. The areas surrounding Bille and Bonny Island have extensive mangroves, with the primary economic activities of the communities in these areas concentrated on fishing in this part of the Delta. The geographic area is also the location of several major oil fields, with a high density of active oil wells and associated petrochemical infrastructure, including the Bonny Oil Terminals which are the main oil export point on the Atlantic coast for transportation of crude oil out of the Niger Delta to importing countries in the West. Indeed, Rivers State itself is one of the major oil-producing states in the Niger Delta, producing ∼20% of Nigeria's estimated daily production of 1.476 million barrels of crude oil per day [22]. Many of the largest global petrochemical corporations are or have been active in the region including Shell, Gulf Oil, Agip, Mobil and Chevron since the 1960s.

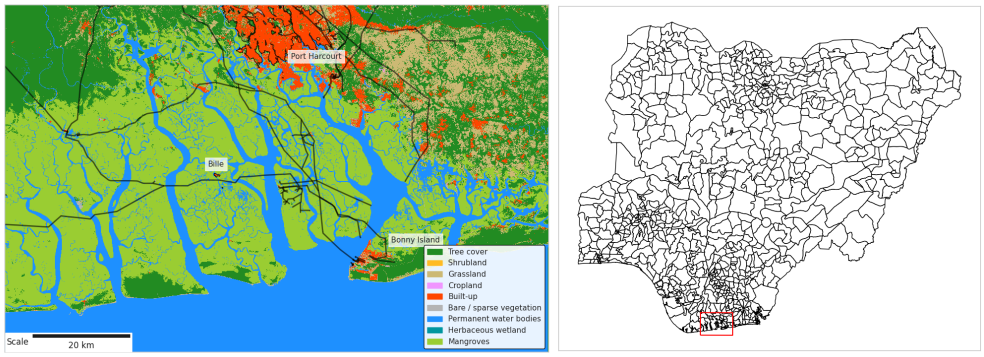

Figure 1. ESA land-use and land-cover map of the region of interest on panel one, with Bille, Bonny Island, and Port Harcourt labelled and pipeline infrastructure overlaid for reference. In the second panel is the FAO GAUL global administrative sub-state boundaries map of Nigeria, where the region of interest is outlined in red.

2. Data

2.1. Sentinel-1

SAR data from the Sentinel-1 A mission (2016–2023) were sourced and pre-processed through Google Earth Engine (GEE) [23], offering dual-polarization backscatter data at a temporal resolution of 6 days and 10-m spatial resolution (Table 1). Optical data from Landsat and Sentinel-2 were deemed unsuitable for rigorous analysis due to persistent cloud cover, underscoring the value of SAR for this study.

Table 1. Datasets used in this work, including (as appropriate) the spatial resolution of the mapped products, their associated temporal baselines, and the source in each case.

Data	Resolution	Revisit Time	Date Range	Source
Sentinel-1 Synthetic Aperture Radar Ground Range Detected	10 m	6 days	2016–2024	[23]
Sentinel-2 MSI: MultiSpectral Instrument, Level-2A	10 m	5 days	2018–2023	[23]
ESA WorldCover 10 m v200	10 m	-	2021–2022	[23]
FAO GAUL: Global Unit Layers, Second-Level Administrative Units	-	-	2015	[23]
OpenStreetMaps Vector Data	-	-	-	[24]
NOSDRA Oil Spill Incident Data	-	-	2006–2024	[14]

2.2. Sentinel-2

The use of optical multi-spectral data in this work was largely impaired by the limited availability of cloud-free scenes. However, data from December 2022 and December 2023 were deemed sufficient quality for validation purposes (Table 1).

2.3. OpenStreetMaps and ESA/WorldCover

Water bodies and built-up areas, which may produce a similar SAR backscatter response to barren land, were masked to limit class confusion using the ESA WorldCover resource [25] and OpenStreetMaps (OSM) data [24]. ESA WorldCover provided insufficient detail on small permanent water bodies, specifically small distributaries, hence 'waterways' from OpenStreetMaps were extracted through the QGIS QuickOSM plugin [26] and reprojected to Sentinel-1 resolution to append finer detail to the mask. For built-up areas, a thresholded December 2023 Sentinel-2 composite with the Normalised Difference Built-up Index (NDBI) was applied to capture recent urban expansion [27]. Utilising a more recent built-up mask in this way reduces the impact of urban sprawl on the results, ensuring that the majority of urban expansion is not misinterpreted as pollution-induced deforestation.

Additional vector data, including the pipeline infrastructure, oil refineries and terminals, and industrial zones, were obtained from OSM to support our analysis (Table 1).

2.4. Oil Spill Data

Geospatial historical oil spill data, such as location, impacted areas, and spill volumes, were obtained from the National Oil Spill Detection and Response Agency (NOSDRA) (https://nosdra.gov.ng/, accessed on 24 April 2024) (Table 1).

3. Materials and Methods

3.1. Data Preparation

The Sentinel-1 data products used were previously curated within Google Earth Engine and therefore have undergone essential pre-processing, including thermal noise removal, radiometric calibration, terrain correction, and conversion to log-scaled decibels (dB). The Analysis-Ready-Data framework for Sentinel-1A backscatter was then applied using the GEE Python API [28], which includes multi-temporal speckle filtering, border noise correction, and radiometric terrain normalisation. Gray Level Co-occurrence Matrix (GLCM) texture analysis was performed to generate an additional 16 bands, complementing the SAR data with spatial and textural information. This approach is widely used in land-cover classification [29], as it enhances the feature set for pixel-based classification models.

To capture temporal feature variability, we composited each year of data with three statistical methods: median, minimum, and maximum. This resulted in a total of 54 input features, with 18 for each statistical composite, two from VV/VH backscatter intensity bands and the remaining 16 from GLCM analysis.

Training data were acquired through manual inspection of the Airbus high-resolution 30 cm base maps (https://intelligence.airbus.com/imagery/reference-layers/basemap/, Acessed: 19 January 2025). The most recent image available in the region, dated 31 December 2022, was used to outline labelled polygons to extract training pixels from the 2023 composite. Creating labelled polygons on static imagery and applying them to temporally composited test data can introduce class confusion if pixels within the training polygons undergo change during the composite period. To minimise this effect, mixed forest training pixels were selected in the preserved Orashi National Forest away from any mapped pipelines. Standard mangrove pixels were outlined to the East of the study region, where no spills have been reported. The identified bare regions are stable over the composite period as the transition of contaminated land to another class over a year is considered an unphysical transition in the context of forestry. A minimum of 65,000 training pixels were exported per class. A visual key for the classes—Mixed Forest, Standard Mangroves, and Bare Land—is depicted in Figure 2.



Figure 2. A visual representation of the classes, depicting Mixed Forest, Standard Mangroves, and Bare Land from left to right, acquired from Airbus 30 cm basemaps.

3.2. Landcover Classification

At present, the primary open-source Land Use/Land Cover (LULC) product characterised by temporal dynamism is Google's Dynamic World product [30], which leverages the coverage, resolution, and timeliness of Sentinel-2 observations and deep learning to provide near real-time LULC products. However, the utility of such products is severely limited in tropical regions due to cloud cover and illumination constraints.

To address these limitations, a supervised XGBoost classification model was developed, tailored to delineate mangroves, mixed forests, and areas deforested by oil contamination. The model objective was set to `multi:softprob`to enable multiclass classification and retain predicted class probabilities. Hyperparameters were optimised through cross-validation methods, specifically stratified 5-fold cross-validation with *sklearn's Grid Search CV*. In addition, early stopping was included in training to prevent overfitting.

The XGBoost algorithm [31] was chosen for its regularisation techniques that prevent overfitting and consequently produce a more stable and generalisable model. Additional motivation includes the speed and scalability when working with large datasets and the ensemble learning approach, which improves performance compared to individual models.

3.3. Hidden Markov Model

A Hidden Markov Model (HMM) was employed for post-processing, refining the classification by addressing unphysical transitions, reducing spatial noise, and ensuring temporal consistency. HMMs are a powerful framework for improving the accuracy of classification results [32], and have been found to be a useful tool for addressing temporally dynamic multiclass classification problems [33–35]. This application of HMMs reduces abrupt class changes which may be deemed unphysical within the context of the target classes.

The model requires a probability transition matrix, for which values were assigned based on accepted physical phenomena. The transition probability from the bare class to another class within the observation window was assumed to be zero. Standard mangroves were equally likely to remain mangroves or transition to the bare class after a pollution event. The forest class was more likely to remain forest than to transition to the bare class.

This temporal smoothing technique serves the additional purpose of mitigating confusion between the 'mangrove' and 'forest' classes and improving the overall spatial coherence and interoperability. In Figure 3, we present a schematic diagram describing how the various datasets are processed to produce a final classification of land surface types.

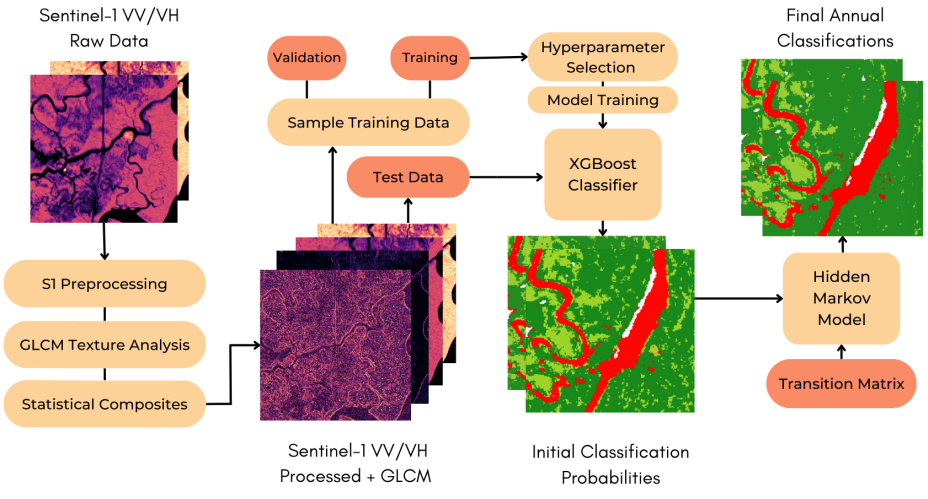

Figure 3. Visual illustration of the main components of the classification workflow, from raw remotely sensed SAR data to the refined annual classification maps, as described in Sections 3.1–3.3.

3.4. Developing a Pipeline Impact Indicator

To analyse the impact region surrounding the pipelines available in the OSM shapefile, a 2.5 km uniform distance buffer was applied per pipeline object. From statistical analysis of the Euclidean distance between each reported spill event epicentre and the nearest pipeline, the mean distance of 852 m with a standard deviation of 1687 m suggests that the majority of spill events occur within this 2.5 km range. Each annual classification was reduced to the area of bare pixels within this buffer. The area within the buffer was calculated using the *pixelArea* function in GEE, paired with a grouped reducer and the per-class values were then converted to hectares. This provided a time series of deforested land changes over time for each pipeline, reduced to its entire length or per specific pipeline segment.

Ordinary Least Squares (OLS) regression was used to analyse degradation rates and assess land-use changes. In this context, the slope (m) represents the degradation rate within the affected area, quantifying the hectares converted to bare land per year. Furthermore, the R^2 value, indicating goodness of fit, provides a means of delineating between 'impulsive' land-use changes and a long-term contaminant-induced increase in bare pixel classification. In Figure 4 we show maps for both R^2 and σ (fraction of non-null pixels) across the region of interest.

Examining the resulting linear fits indicated that these parameters' extreme values were correlated for boundary condition scenarios sampled from sites throughout the Delta evident in Figure 4. Regions most impacted by persistent spills exhibited a more linear trend in the spread of degraded land, likely due to the compound impact of repeated spills in the mangroves. Though the impact on seedlings and a reduction in leaf density can be observed within days in a heavily contaminated area [36], numerous studies indicate more established mangroves typically experience mortality and dieback on a scale of up to 14 years depending on spill severity and mangrove species [37–39]. Additionally, the site deterioration, sediment loss, and erosion that follow the event can cause permanent habitat loss within 30 years [37,38]. Therefore, sites with a stark deviation in trend are more likely to have experienced some human intervention impulse event, such as deforestation for timber production, agricultural land expansion, or settlement expansion. We confirmed this hypothesis following the examination of contemporaneous Sentinel-2 true-colour composite surrounding those pipeline segments exhibiting a low R^2 value. In these composites, we found evidence of deforestation for cropland expansion and small areas of urban sprawl which had not been captured in the built-area mask due to the limitations of using a global land-cover mask from 2021–2022.

A 'Pipeline Impact Indicator' (PII) was constructed using the compiled regression statistics to capture the severity of degradation for each location using the best-fit slope (m), R^2 and the fraction of non-null pixels within the delineated buffer area (defined here as σ). A Min-Max Scaler was applied to the slope to scale the data distribution and produce an indicator between 0 and 1 for ease of interpretation within the frame of reference. When applied at the entire pipeline extent scale, the slopes were not normalised to the measured area, as this produced a biased weighting towards the shortest sections of the pipeline compared to the more extensive sections with broader impact. Consequently, short pipeline sections with high impact relative to their small impact area were not well represented in this implementation of the PII. This limitation motivated the implementation of the PII at a more granular scale, where normalising to the measured area would not skew results. This approach yielded two mapped representations of the PII, the entire pipeline length and at segmented pipeline scales.

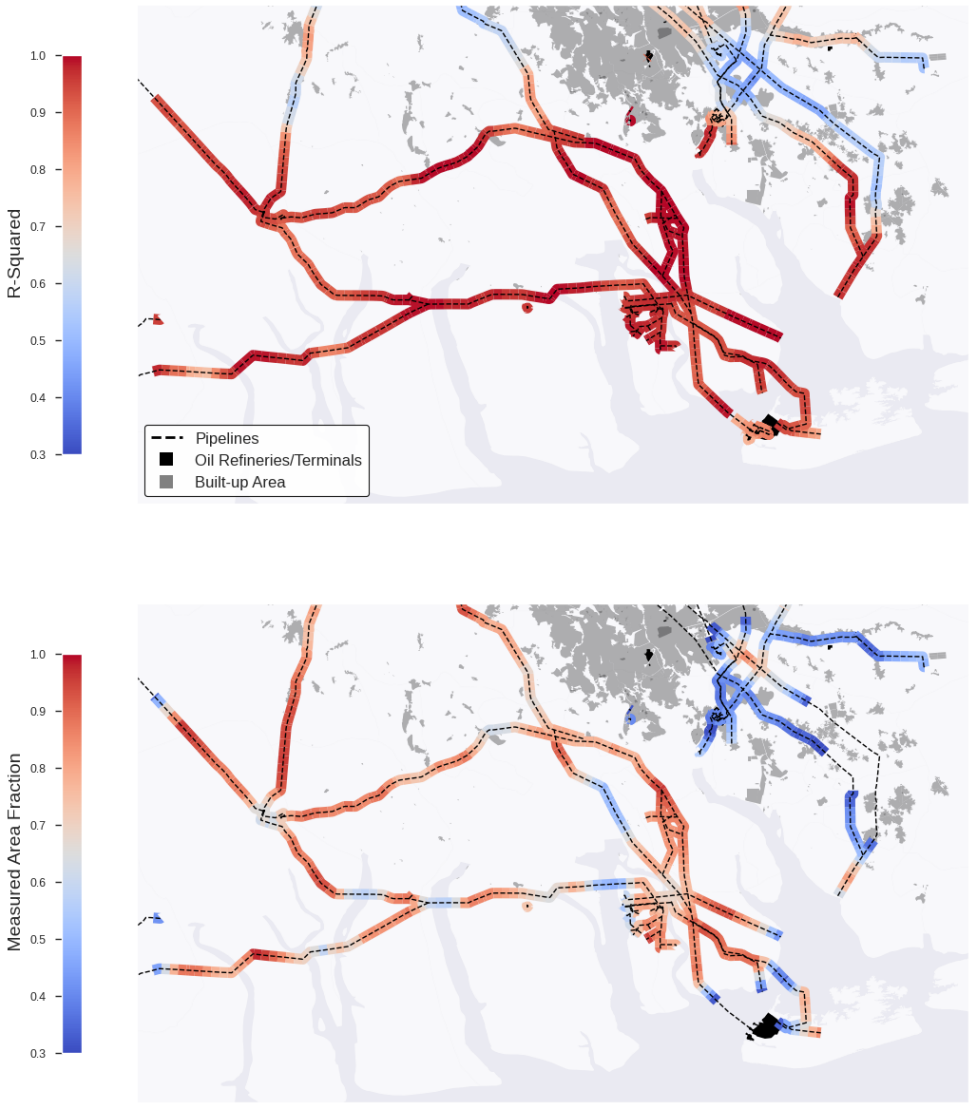

Figure 4. Spatial distribution of the R^2 and σ parameters discussed in Section 3.4. The top panel shows the distribution of R^2 values, where the lower extremes are proximal to urban areas, where urban sprawl and cropland expansion influence the linear fit due to misclassified anthropogenic expansion. Similarly, the bottom panel shows the distribution of σ values—the fraction of non-null pixels within the delineated buffer area—where regions near urban areas and waterbodies are heavily masked.

Additionally, the "fraction of non-null pixels" σ parameter was introduced to filter out areas with heavy masking (e.g., large water bodies or urban zones). This filters out heavily masked regions from the forestry impact analysis, as these alternate land-cover areas cannot be assessed with the same degree of confidence for urgent intervention needs. A threshold of 0.3 for the non-null fraction was set to exclude areas with insufficient classified data, ensuring there is sufficient classified area to produce reliable, relevant, and statistically robust results.

We define the Pipeline Impact Indicator as

$$PII = mR^2 \tag{1}$$

where m and R^2 represent the slope and R-squared value, respectively, as previously described. Combining these two time-series descriptors produces an indicator between 0 and 1, capturing both the rate of change and a proxy for confidence that a spill event

is driving the land-cover changes. When R^2 approaches zero at this granular scale, the time series likely includes 'impulse' events, as we have previously described (localised deforestation and/or urban sprawl), where the sharp deviations from the local trend are not representative of the behaviour of mangroves under pollution stress observed throughout the Delta. This method for interpreting the classification results over the study period does introduce a limited capacity for capturing the impact of a non-linear degradation effect. Although such an impact was not observed at the temporal scale of this study, if the workflow were implemented at a higher time frequency, it may be possible to observe the impact of a large spill on unestablished vegetation. There would be an increase in computational cost, but it would be possible to monitor the region at the current Sentinel-1 repeat cycle of ∼6 days. However, this would also require more robust and temporally dynamic land-use classification masks to eliminate the misclassification of anthropogenic expansion for pollution-induced deforestation.

4. Discussion of Results

4.1. Land Classification Model Evaluation

During the model evaluation, emphasis was placed on precision, recall, and the F1-score metrics, prioritising these over accuracy in isolation. As presented in Table 2, the final model demonstrated robust performance across all classes—Figure 5 illustrates the classification results against contemporaneous imagery from Sentinel-1 and Sentinel-2 over three distinct regions. Particular emphasis was placed on the 'bare' class, where both high precision and recall were critical to accurately detect deforested and degraded land.

Table 2. Classification accuracy assessment results.

Class	Precision	Recall	F1-Score
Bare	0.97	0.93	0.95
Standard mangroves	0.92	0.88	0.90
Tall mangroves/mixed forest	0.86	0.92	0.89

The 'Standard Mangroves' and 'Tall Mangroves/Forest' classes exhibited some degree of class ambiguity, as expected, due to the natural overlap and intermixing of mangrove species and forest ecosystems. This is further highlighted in the confusion matrix in Figure 6, where the most significant misclassification rates are between these two classes. A train-test split of (0.7, 0.2, 0.1) was used for training, testing, and validation, respectively. An overall accuracy of 90.56% was achieved with the validation set, underscoring the generalisation of the model given the 90.61% accuracy in the test set.

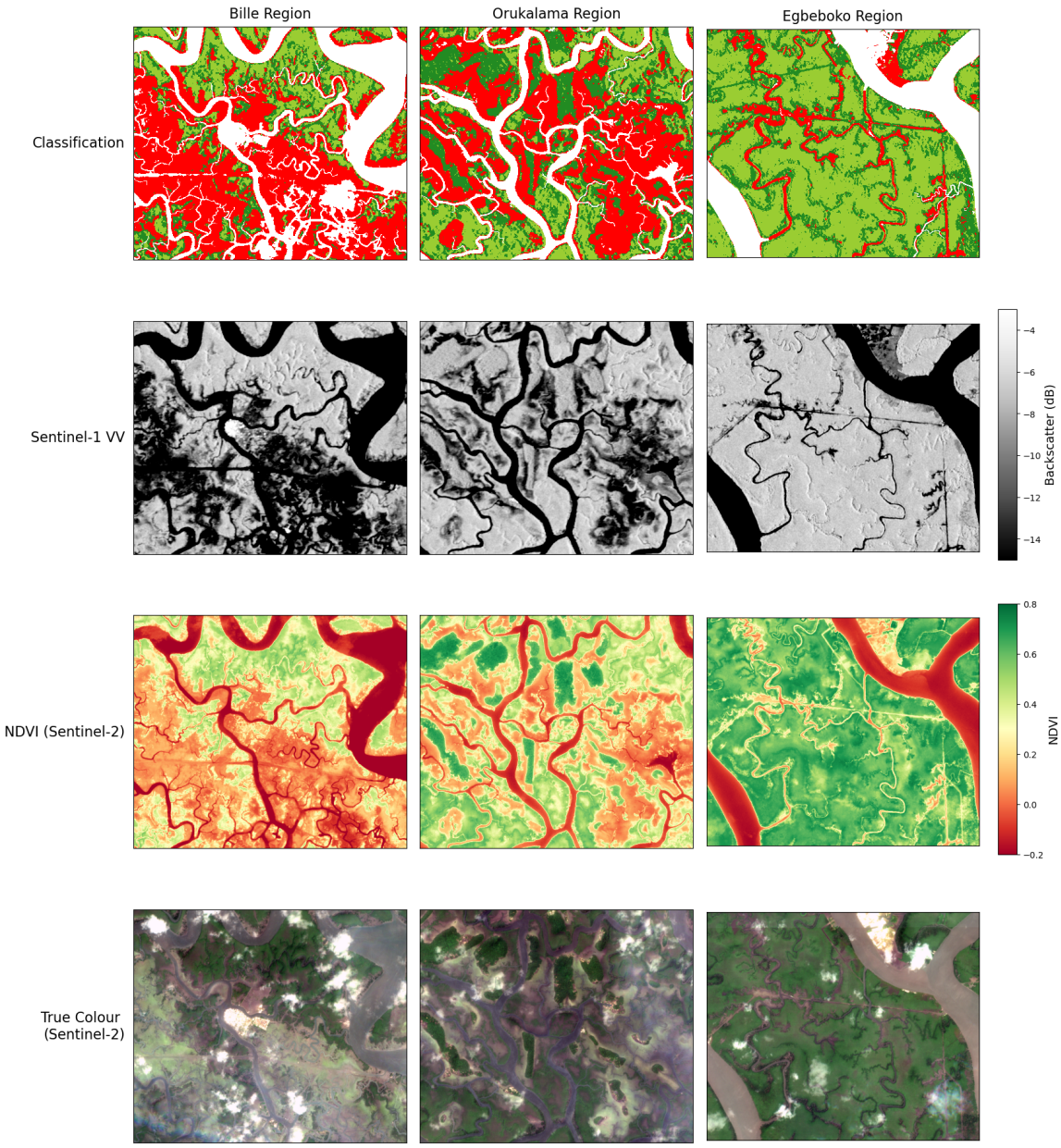

Figure 5. Comparative visual of classification results against co-occurring Sentinel-1 and Sentinel-2 images from December 2023. The first row of data are patches of classification results for three distinct regions. Here red represents the bare land class, green represents standard mangroves, and forest green represents the standard forests. The white areas were identified as masked classes such as urban areas and were not classified. The second row illustrates Sentinel-1 VV backscatter, one band of the model inputs. The third and final rows are Sentinel-2 data are for comparative purposes. Here NDVI is used as a good proxy for vegetation health, where the red areas represent sparse to no vegetation. The final row shows a True Colour Composite of the region.

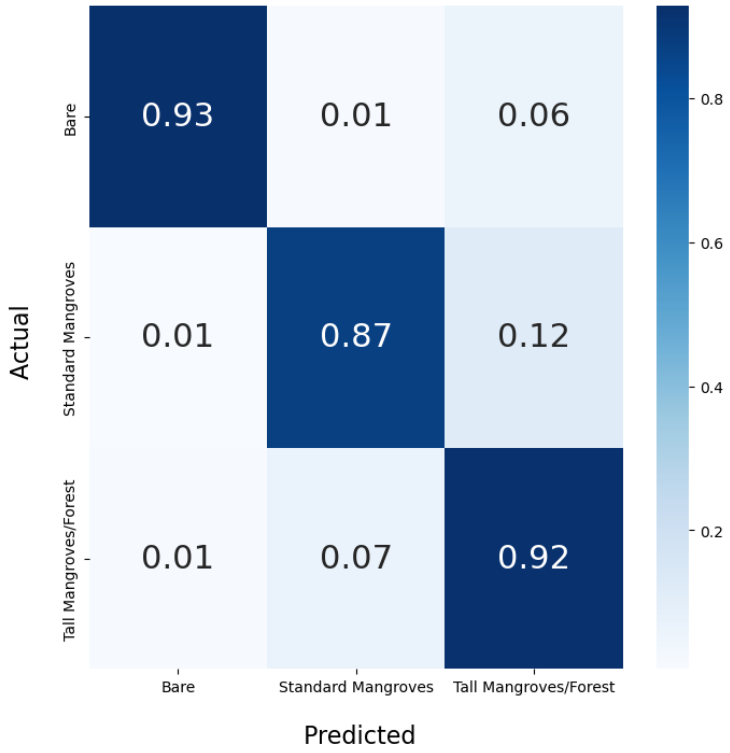

Figure 6. Model confusion matrix for validation set. Values are normalised to show the proportion accurately classified in each class.

4.2. Regional Scale Analysis

4.2.1. Ecological Degradation Effects in Rivers State Region

An examination of Figure 7 reveals several epicentres of ecological degradation in the Rivers State region, most likely driven by compounded oil spills over this time. From a regional scale linear regression fit in Figure 8, we can estimate that the total bare land area is increasing at a rate of 5644 hectares/year. Although it is unlikely that it will continue to expand at this rate over the next 25 years, to eradicate the remaining 130,000 hectares of mangrove area classified by our analysis in this region, the threat of significant, irreversible damage is clear unless more effective remediation efforts are implemented, or the rate of spread is reduced.

Ongoing dredging and channel widening operations in the region—intended to improve accessibility to oil reserve zones—have led to the classification of certain water bodies as bare on the banks. This misclassification occurs due to sulfidic dredged materials being dumped along the banks, resulting in mangrove suffocation through soil acidification and heavy metal pollution [40]. The presence of some of these waterbodies, previously absent in the initial mask, has become more apparent as vegetation density decreases. Despite these activities, the final waterbody mask was deemed sufficient for the objectives of this study as adding a water class would reduce class certainty.

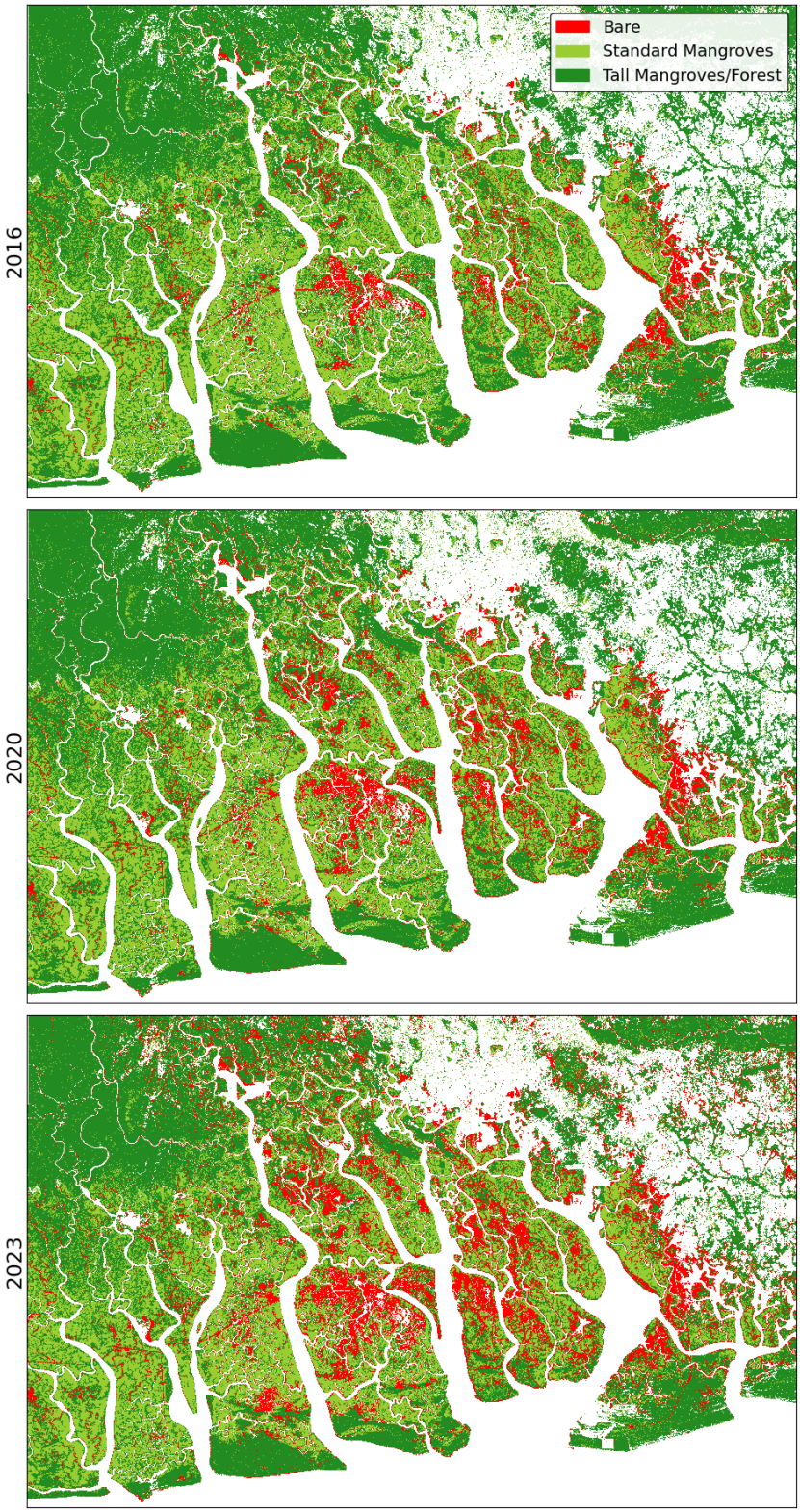

Figure 7. Annual post-HMM classification of Rivers State region for 2016, 2020, and 2023. Cropland, grassland, permanent water bodies, and built-up areas are all masked out in white. The classification results shown here highlight the spatial distribution of land degradation, with several epicentres of ecological deterioration becoming increasingly apparent.

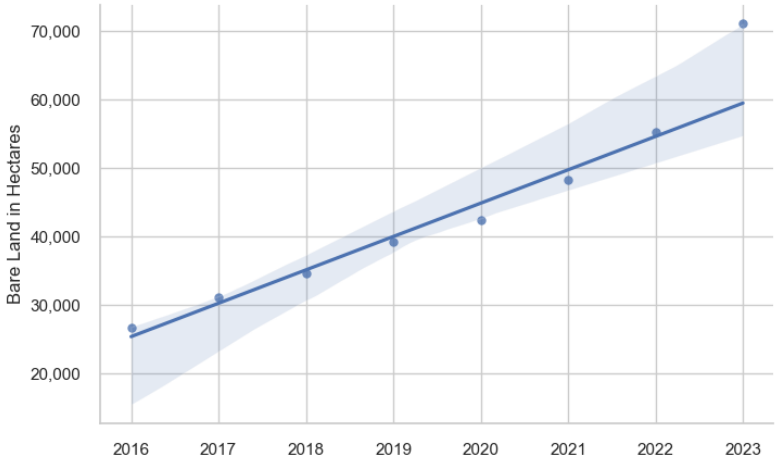

Figure 8. Linear regression of the annual classification of bare land measured in hectares across the full study region, where the blue region is the 95% confidence interval of the linear fit.

4.2.2. Oil Spill Impacts in Rivers State Region

Figure 8 indicates that at the state scale, the present remediation and clean-up operations are ineffective in slowing the expansion rate of bare land and land subsidence in the region. The measured area in 2023 exceeds the 95% confidence interval of the linear fit, likely as a result of the unprecedented quantity spilled in the region in 2022, as shown in Figure 9. The largest of these spills involved 26,000 barrels of oil over a two-month period, during which only 810 barrels were reportedly recovered. As the spill occurred in a tidal zone over a long period, the spill had most likely spread throughout the Delta before more could be recovered and contributed to extensive damage that was apparent over an extended area within this two-year period. Further detailed in the corresponding spill report are the affected properties, which include surface water and vegetation impacted by oil staining, and observations of withering vegetation [14].

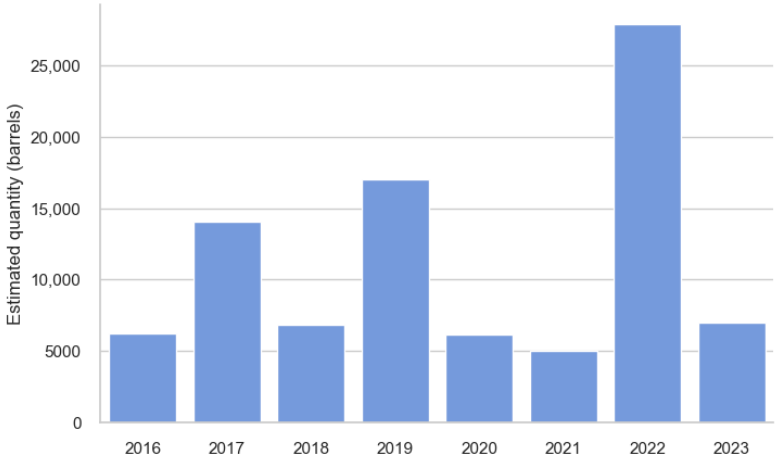

Figure 9. Total quantity spilt annually in the region as reported by NOSDRA [14].

For a more localized environmental impact assessment, we analysed oil spill data from the Nigerian Oil Spill Monitor database [14]. Though it has been noted that many of the occurrences in the province are under-reported, these data nevertheless provide critical context for understanding the accelerated rate of mangrove decline in specific areas. As illustrated in Figure 10, there is a high frequency of low-quantity spills along the pipelines in the Port Harcourt area. While these spills have resulted in the degradation of the mangroves to the Southern end of the pipeline, the damage to the surrounding

agricultural land would be of more relevance to this area. However, quantifying the impact on agricultural land was not feasible in this study due to the unavailability of open-access, high cadence, and high-resolution multi-spectral observations, required to overcome cloud cover challenges and the small parcel size.

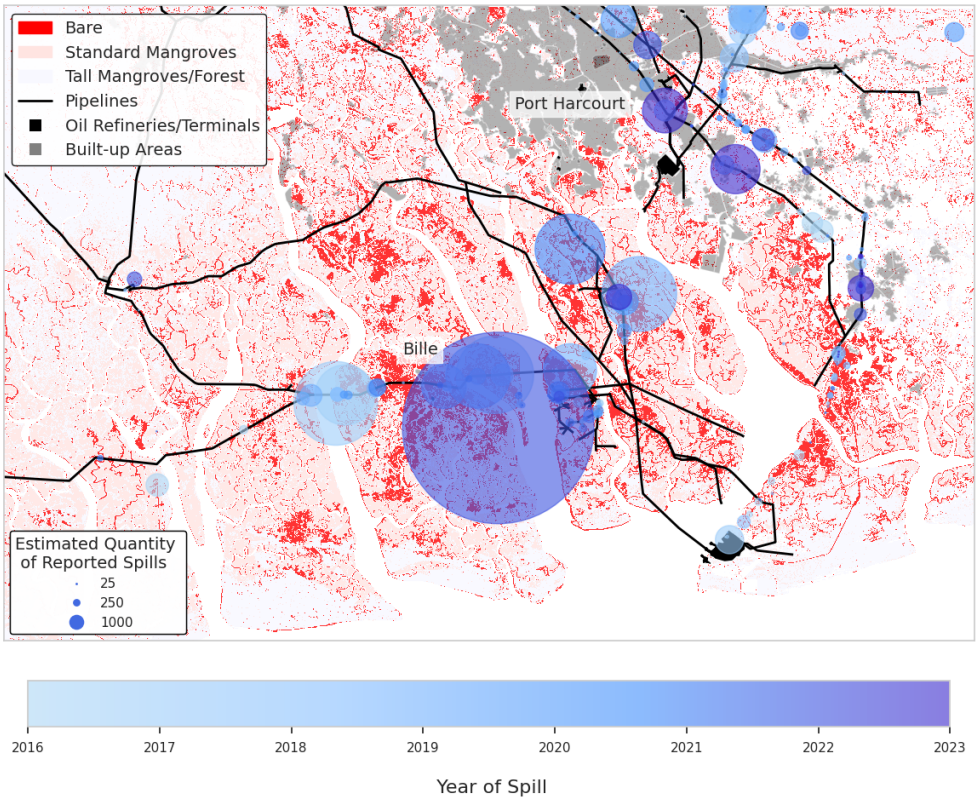

Figure 10. Classification results for the year 2023 overlaid with key features including pipeline infrastructure, built-up areas, oil refineries, and terminals. Spill locations from [14] are also illustrated with the size of each circular spill marker, indicating the estimated quantity and the colour denoting the reported date of the spill. This figure illustrates the spatial and temporal distribution of the reported oil spills during the study period.

The central peninsula surrounding Bille, west of Bonny Island, has experienced some of the largest oil spills in recent years. The impact of these spills is evident in the concentration of land degradation shown in Figure 7. We examine this area in more detail in the next section through the lens of our Pipeline Impact Indicator.

4.3. Pipeline Scale Analysis

Pipeline Impact Indicator

The speed and direction of water flow within the Delta impact the distribution of oil following a spill incident. If clean-up efforts are delayed, the flow dynamics of the Delta are likely to cause a more prolonged and widespread impact. As the mangroves are predominantly found in the coastal vegetation region, the surrounding water bodies have a complex repetitive tidal cycle rather than a unidirectional flow. Over time, this estuarine environment becomes a persistent sink for the petroleum hydrocarbons in crude oil, constantly redistributing through sediments and on the water surface rather than flushing the contaminants out to sea [41]. However, the immediate vicinity of the spill is likely to experience the most severe damage as the concentration of oil will be higher in that region initially, particularly given the hydrophobicity of many hydrocarbons [42].

Oil spill data alone are unreliable as a metric to evaluate the environmental impact of pipeline infrastructure due to the need for thorough and timely reporting. It is well-documented that there is great uncertainty regarding data veracity and complete spill reports in the Niger Delta [43]. The self-reporting aspect demanded by regulatory compliance brings into question a conflict of interest and leads to reports that are incomplete, inconsistent, or incoherent. It is also clear that the resources required to cross-examine reports are a point of contention amongst analysts who are working towards transparency in the industry. Though the availability of reports through a public resource such as NOSDRA [14] is certainly to be commended, discrepancies of the order of 15–20% between publicly available data and international oil company published statistics [43] have been reported. Research built entirely upon such large uncertainty calls for more independent and objective methods of assessing the impact of spills in the region.

To address this, we developed the Pipeline Impact Indicator (PII) to quantify the impact based on the rate of bare land increase within a 2.5 km buffer of each pipeline, a buffer size supported by spill locations from [14] and the Euclidean distance analysis detailed in Section 3.4. The PII maps, shown in Figure 11, provide a more objective metric for identifying pipeline segments with accelerated environmental damage. This section will discuss four instances of each implementation of the PII, chosen specifically to characterise the minimum and maximum values, as well as two additional examples that are of interest given the regional context. These results are detailed in Table 3.

Table 3. PII results for all sample pipelines segments labelled in Figure 11.

Segment Label	PII
Pipeline 1	0.18
Pipeline 2	0.78
Pipeline 3	0.99
Pipeline 4	0.21
Zone A	0.06
Zone B	0.84
Zone C	0.54
Zone D	0.86

The PII revealed varying levels of impact across different pipelines and pipeline buffer regions, as we show in Figures 12 and 13. For instance, sample pipeline 1 (southwest of Bille) marked in Figure 11 (top panel), has a low PII of 0.18, corresponding to the relatively small number of spills and the limited extent of bare land per unit of affected area. In contrast, pipeline segment 2, which runs through Bille, exhibited a much higher PII of 0.78, indicating substantial damage which we originally identified in our regional classification map as being associated with the largest quantity of oil spills within a 2.5 km radius of its associated pipeline infrastructure (Figure 7). This area has been exposed to a large accumulated quantity of crude oil spillages relative to the length of the infrastructure component. This area had already suffered from significant pollution-induced deforestation at the start of this study, so while bare land expansion continued, its rate was lower than in newly contaminated regions. The existing contamination limits the measurable impact of new spills on mangrove forests, as much of the affected area was already devoid of vegetation at the time of detection. Sample pipeline 3 had the highest PII rating at 0.99, marking it as an area in urgent need of intervention and reflecting the total quantity of spills distributed over this longer infrastructure segment. This pipeline's location showed little degradation at the beginning of this study, but the sudden increase in pollution during the study period led to rapid degradation of surrounding land, demonstrating the widespread impact associated with the onset of significant pollution activity, as seen in Figure 13.

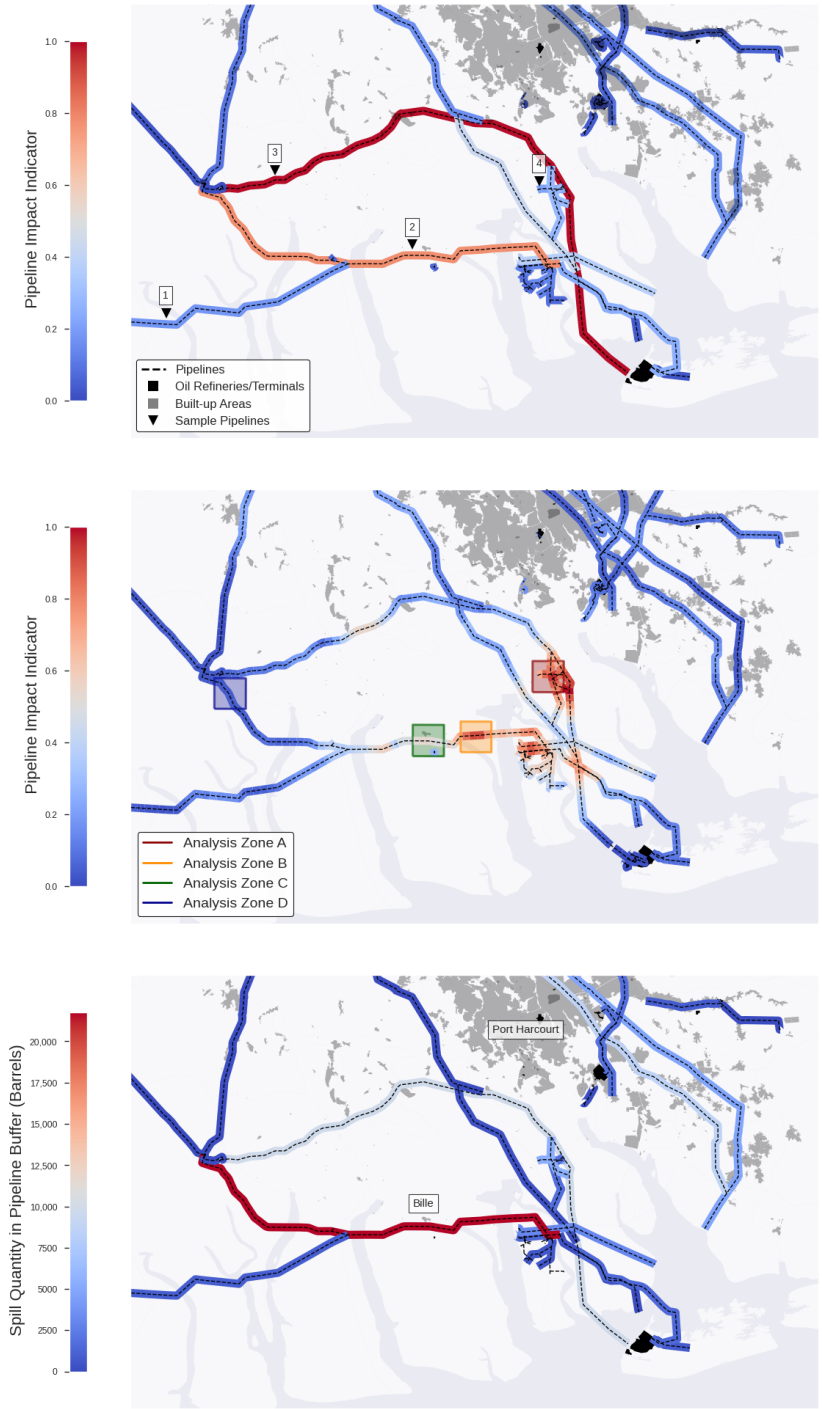

Figure 11. The top panel shows the initial implementation of the Pipeline Impact Indicator (PII). Four sample pipelines are numbered in this plot, which are expanded upon in Figure 12 and represent the range of values in this PII implementation at the total pipeline extent scale. The centre panel shows the PII assessment at a more granular scale of 1 km of pipeline per segment, highlighting regions of significant impact for targeted intervention. In the centre panel, four regions of comparison are outlined to illustrate the range of PII values and are further expanded upon in Figure 13. The bottom panel shows the estimated spill quantity data from (NOSDRA, 2006) to within 2.5 km of the nearest pipeline, with Bille and Port Harcourt labelled for reference. This figure collectively provides a comprehensive view of the environmental impact associated with specific segments of petrochemical pipeline infrastructure, highlighting those sections of the pipeline with accelerated and significant impact on adjacent mangrove forest decline.

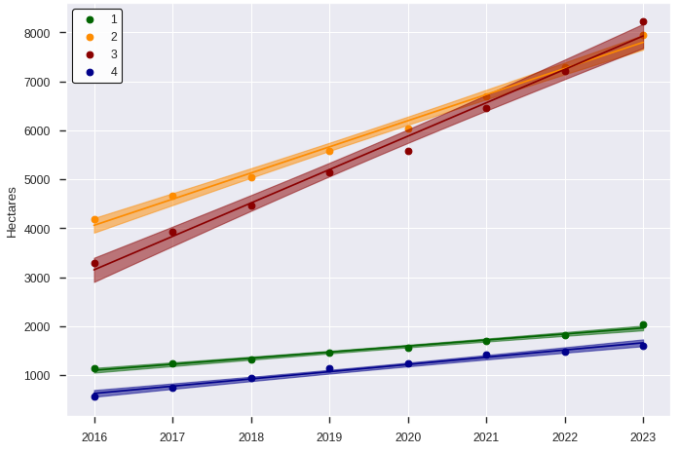

Figure 12. Linear regression fit of the bare land increase for sample pipelines labelled in the top panel of Figure 11. This figure emphasises the discrepancy between pipelines exerting significant stress on adjacent mangrove forest health, with pipelines 2 and 3 showing a widespread deterioration effect. Conversely, pipelines 1 and 4 do not show the same impact in terms of the overall extent of deterioration.

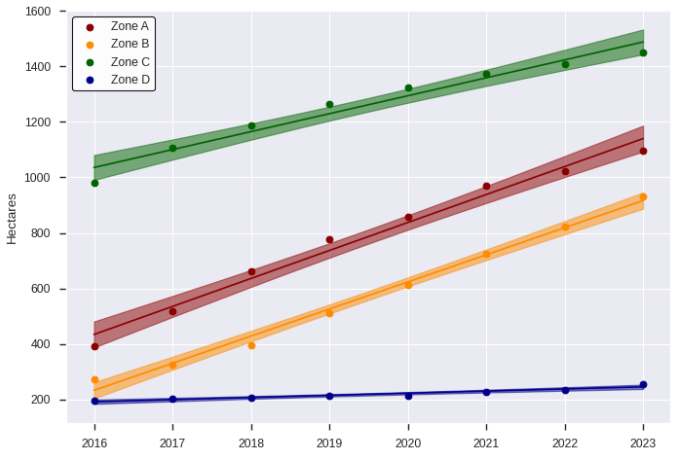

Figure 13. Linear regression fit of the bare land increase within the pipeline segment buffer of the four zones labelled in the central panel of Figure 11. This plot illustrates the higher degradation rate in Zone B (East of Bille), compared to Zone C, despite the former having less degraded forest area at the onset of the study period, capturing the impact on a previously unaffected area. The results also highlight Zone D as comparably stable throughout the study period.

Given the extensive pipeline network in Rivers State, which spans more than 600 km, it is essential to assess the environmental impact at a more granular scale. Our approach identifies pipeline infrastructure hotspots and associated locations where contamination damage is most significant and can enable targeted maintenance and improved safeguards against sabotage and oil bunkering.

For instance, Figure 11 (centre panel) presents an analysis of the pipelines in 1 km increments, highlighting several areas of interest for further inspection. The infrastructure segment east of Bille (Zone B) shows a high PII rating of 0.84, significantly surpassing the rating for Zone C (0.54), which overlaps with the town of Bille itself. Despite the extensive area of degraded land surrounding Bille, observed in Figure 7, the PII reveals a higher spread rate in Zone B, suggesting recent spills contributing to the increased spread rate or severe long-term impact spreading from the epicentre of the original affected area (Figure 13). The urgency of intervention in Zone B is evident, particularly for areas such as the Touma Mangrove Forest, which is now at critical risk of degradation. This area

again illustrates the degradation expansion associated with the impact on a previously unaffected area.

In contrast, the western portion of the Bille pipeline (Zone D) shows minimal impact on the surrounding environment over the 8-year study period. This is reflected in the PII's low rating for this zone, contrasting sharply with areas of more severe degradation and this is further supported by the absence of reported spills in the region. It is also important to acknowledge that Zone A, which also contains sample pipeline 4 in the top panel of Figure 11, has a distinctly higher rating at a granular scale as opposed to the pipeline extent scale. Though this pipeline has a small total impact area, it has a similar spread rate to Zone B, which has been suggested as a region in need of urgent intervention. This underscores the utility of evaluating pipeline impact at a more granular scale, as a pipeline with a small footprint may still contain sections with significant degradation rates, warranting closer inspection and targeted intervention.

It is also noteworthy that segments of pipeline 3 north of Bille, which had no reported spills during this study, showed unexpectedly high PII values. Further examination using Sentinel-2 RGB composites from 2023 revealed no clear evidence of anthropogenic drivers such as deforestation for agriculture or logging, nor did it show a spatial pattern consistent with such activities. This suggests the possibility of under-reporting or perhaps of oil-bunkering activities contributing to the pollution-induced deforestation observed in these areas.

5. Conclusions

Multiple studies have documented the damage to mangrove forests caused by petrochemical activities [44–47]. Together, these studies indicate that crude oil spillages play a significant role in damaging fragile mangrove ecosystems, with associated debilitating impacts that persist for decades [48]. Traditional methods for tracking changes in mangrove biomass health typically require vegetative indices, most notably NDVI, to form the basis for these analyses [49–51]. However, such sensor modalities are compromised by the effects of cloud cover, which tends to dominate the meteorological conditions in the tropical/subtropical locations associated with mangrove forests. This limitation compromises the ability of such studies to apply a more precise and timely means of quantifying change.

The growing availability of analysis-ready data products from active sensor missions, particularly the European Union's Copernicus Sentinel-1 mission, provides a weather-independent means of directly quantifying structural variations in mangroves every $\sim$6 days with a spatial resolution of $\sim$10 m. Several studies have integrated Sentinel-1 and other SAR mission data into programmes to successfully map mangrove forests [52–54], demonstrating the efficacy of this modality in such a general application.

The novelty of our work lies in the development of a workflow that enables the study of the immediate mangrove environment proximal to petrochemical pipeline infrastructure over time, where we demonstrate "our proof of concept" in the River States region of the Niger Delta. Additionally, our workflow is weather-independent and can monitor large areas at a much lower cost, overcoming the limitations of traditional methods. Using our empirically derived 'Pipeline Impact Indicator' (PII), reported spillage events can be associated with proximal mangrove impact, and the rate of such mangrove damage can be quantified spatiotemporally. Our analysis has identified regions where targeted remediation efforts need to be actively implemented by responsible stakeholders and where intervention would be most effective in reducing the spread of oil pollution-induced mangrove loss. Furthermore, specific oil pipeline locations for which there have been no documented spillage events, yet which show all the signatures of such an event as having taken place, have been identified in our analysis.

The lack of effective policy to address the under-reporting of oil spills and mitigate persisting pollution has resulted in severe environmental, socio-economic, and cultural consequences for the Niger Delta. This underscores the urgent need for a critical review of existing pollution mitigation and remediation policies in the region. An effective mitigation and remediation policy must include objective and efficient methods for monitoring spill sites, quantifying the magnitude of pollution events and assessing the impact on the surrounding ecosystems. This study proposes a workflow to lay the foundation for transparent, comprehensive, and efficient monitoring systems to assess the environmental impact of oil pollution on the mangrove ecosystem and other vital ecosystems. Such monitoring systems can support the development of effective mitigation and remediation policies to address the adverse impacts in the Niger Delta region and other affected regions worldwide.

Our study further demonstrates the significant potential of incorporating high-resolution SAR Earth Observation data to enable independent monitoring of the operational integrity of petrochemical infrastructure located in ecologically sensitive environments, overcoming the established constraints of site accessibility and the cost associated with scaling evaluation temporally and spatially. Our novel methodology responds to the urgent need for scalable, continuous environmental monitoring to provide stakeholders with the data and evidence needed to prioritise intervention and inform policy.

Author Contributions: Contribution to the paper is as follows: J.O., D.O., M.G., A.G. and A.O.B. contributed to the conceptualisation of the research goals and methodology, A.O.B. provided qualitative data, J.O. conducted data curation, formal analysis, investigation, visualisation, and validation, P.C. conducted project management and coordination throughout, P.C.M. provided a critical review of the methods and workflow, A.G. and C.S. acquired funding and were responsible for the overall project, A.G. provided supervision throughout planning and execution. All authors have read and agreed to the published version of the manuscript.

Funding: This study was supported by the Science Foundation Ireland (SFI) Future Innovator Prize: AI for Societal Good Challenge, under Grant Number 19/FIP/AI/7515P.

Data Availability Statement: The original contributions presented in this study are included in the article. The original contributions presented in the study are included in the article, further inquiries regarding workflow scripts and data products can be directed to the corresponding author.

Conflicts of Interest: The authors declare no conflicts of interest.

References

1. Ansah, C.E.; Abu, I.O.; Kleemann, J.; Mahmoud, M.I.; Thiel, M. Environmental Contamination of a Biodiversity Hotspot—Action Needed for Nature Conservation in the Niger Delta, Nigeria. *Sustainability* **2022**, *14*, 14256. [CrossRef]
2. Hai Hoa, N.; Tri Son, H.; Thi Linh, N.; Ojeda de Vicent, D.; Ngoc Linh, N. Using planetscope data to estimate carbon sequestration of mangrove forests: A case study in Tien Yen district, Quang Ninh province. *J. For. Sci. Technol.* **2023**, *8*, 087–099. [CrossRef]
3. UNDP. Human Development Report: Niger Delta Human Development Report. 2006. Available online: https://hdr.undp.org/content/human-development-report (accessed on 2 December 2024).
4. Babatunde, A.O. Local perspectives on food security in Nigeria's Niger delta. *Extr. Ind. Soc.* **2020**, *7*, 931–939. [CrossRef]
5. Odioko, E.; Becer, Z.A. The economic analysis of the Nigerian fisheries sector: A Review. *J. Anatol. Environ. Anim. Sci.* **2022**, *7*, 216–226. [CrossRef]
6. Babatunde, A.O. Oil exploitation and food insecurity in Nigeria's Niger Delta. *J. Mod. Afr. Stud.* **2023**, *61*, 165–187. [CrossRef]
7. Tuttle, M.L.; Charpentier, R.R.; Brownfield, M.E. *The Niger Delta Petroleum System: Niger Delta Province, Nigeria, Cameroon, and Equatorial Guinea, Africa*; US Department of the Interior: Washington, DC, USA; US Geological Survey: Reston, VA, USA, 1999.
8. Mafiana, M.O.; Bashiru, M.D.; Erhunmwunsee, F.; Dirisu, C.G.; Li, S.W. An insight into the current oil spills and on-site bioremediation approaches to contaminated sites in Nigeria. *Environ. Sci. Pollut. Res.* **2021**, *28*, 4073–4094. [CrossRef]
9. Ukhurebor, K.E.; Ngonso, B.F.; Egielewa, P.E.; Cirella, G.T.; Akinsehinde, B.O.; Balogune, V.A. Petroleum spills and the communicative response from petroleum agencies and companies: Impact assessment from the Niger Delta Region of Nigeria. *Extr. Ind. Soc.* **2023**, *15*, 101331. [CrossRef]

10. United Nations Environment Programme (UNEP) Environmental Assessment of Ogoniland. 2011. Available online: https://www.unep.org/resources/report/environmental-assessment-ogoniland (accessed on 19 January 2025).
11. Fentiman, A.; Zabbey, N. Environmental degradation and cultural erosion in Ogoniland: A case study of the oil spills in Bodo. *Extr. Ind. Soc.* **2015**, *2*, 615–624. [CrossRef]
12. Nwaichi, E.O.; Osuoha, J.O. Has the National policy on environmental pollution control in Nigeria been neglected in the Niger Delta region? An update. *Environ. Dev. Sustain.* **2022**, *24*, 12494–12517. [CrossRef]
13. Sam, K.; Pegg, S.; Oladejo, A.O. Mining from the pipeline: Artisanal oil refining as a consequence of failed CSR policies in the Niger Delta. *J. Environ. Manag.* **2024**, *352*, 120038. [CrossRef]
14. NOSDRA. Nigerian Oil Spill Monitor. 2006. Available online: https://nosdra.oilspillmonitor.ng/index.html (accessed on 19 January 2025).
15. Kostianoy, A.G.; Lavrova, O.Y.; Solovyov, D.M. Oil Pollution in Coastal Waters of Nigeria. In *Remote Sensing of the African Seas*; Springer: Dordrecht, The Netherlands, 2014; pp. 149–165. [CrossRef]
16. Okafor-Yarwood, I. The effects of oil pollution on the marine environment in the Gulf of Guinea—The Bonga Oil Field example. *Transnatl. Leg. Theory* **2018**, *9*, 1–18. [CrossRef]
17. Amnesty International. Bad Information: Oil Spill Investigations in the Niger Delta. 2013. Available online: https://www.amnesty.org/en/documents/afr44/028/2013/en/ (accessed on 2 December 2024).
18. Obida, C.B.; Blackburn, G.A.; Whyatt, J.D.; Semple, K.T. Counting the cost of the Niger Delta's largest oil spills: Satellite remote sensing reveals extensive environmental damage with >1million people in the impact zone. *Sci. Total Environ.* **2021**, *775*, 145854. [CrossRef]
19. Ordinioha, B.; Brisibe, S. The human health implications of crude oil spills in the Niger delta, Nigeria: An interpretation of published studies. *Niger. Med. J. J. Niger. Med. Assoc.* **2013**, *54*, 10–16. [CrossRef] [PubMed]
20. Giuliani, G.; Camara, G.; Killough, B.; Minchin, S. Earth Observation Open Science: Enhancing Reproducible Science Using Data Cubes. *Data* **2019**, *4*, 147. [CrossRef]
21. Rostan, F.; Riegger, S.; Huchler, M.; Croci, R.; Torres, R. The Sentinel-1 C-SAR instrument. In Proceedings of the EUSAR 2012; 9th European Conference on Synthetic Aperture Radar, Nuremberg, Germany, 23–26 April 2012; pp. 166–169.
22. OPEC Annual Statistical Bulletin, 2023. Available online: https://publications.opec.org/asb/chapter/show/123/2165/2175 (accessed on 19 January 2025).
23. Gorelick, N.; Hancher, M.; Dixon, M.; Ilyushchenko, S.; Thau, D.; Moore, R. Google Earth Engine: Planetary-scale geospatial analysis for everyone. *Remote Sens. Environ.* **2017**, *202*, 18–27. [CrossRef]
24. OpenStreetMap contributors, *Planet dump retrieved from* https://planet.osm.org, 2017. Available online: https://www.openstreetmap.org (accessed on 19 January 2025).
25. Zanaga, D.; Van De Kerchove, R.; Daems, D.; De Keersmaecker, W.; Brockmann, C.; Kirches, G.; Wevers, J.; Cartus, O.; Santoro, M.; Fritz, S.; et al. ESA WorldCover 10 m 2021 v200. 2022. Available online: https://esa-worldcover.org/en/data-access (accessed on 19 January 2025).
26. Trimaille, E. QuickOSM. 2022. Available online: https://github.com/3liz/QuickOSM (accessed on 19 January 2025).
27. Xu, R.; Liu, J.; Xu, J. Extraction of High-Precision Urban Impervious Surfaces from Sentinel-2 Multispectral Imagery via Modified Linear Spectral Mixture Analysis. *Sensors* **2018**, *18*, 2873. [CrossRef] [PubMed]
28. Mullissa, A.; Vollrath, A.; Odongo-Braun, C.; Slagter, B.; Balling, J.; Gou, Y.; Gorelick, N.; Reiche, J. Sentinel-1 SAR Backscatter Analysis Ready Data Preparation in Google Earth Engine. *Remote Sens.* **2021**, *13*, 1954. [CrossRef]
29. Kupidura, P. The Comparison of Different Methods of Texture Analysis for Their Efficacy for Land Use Classification in Satellite Imagery. *Remote Sens.* **2019**, *11*, 1233. [CrossRef]
30. Brown, C.F.; Brumby, S.P.; Guzder-Williams, B.; Birch, T.; Hyde, S.B.; Mazzariello, J.; Czerwinski, W.; Pasquarella, V.J.; Haertel, R.; Ilyushchenko, S.; et al. Dynamic World, Near real-time global 10 m land use land cover mapping. *Sci. Data* **2022**, *9*, 251. [CrossRef]
31. Chen, T.; Guestrin, C. XGBoost: A Scalable Tree Boosting System. In Proceedings of the 22nd ACM SIGKDD International Conference on Knowledge Discovery and Data Mining, San Francisco, CA, USA, 13–17 August 2016; Krishnapuram, B., Shah, M., Smola, A.J., Aggarwal, C., Shen, D., Rastogi, R., Eds.; ACM: New York, NY, USA, 2016; pp. 785–794. [CrossRef]
32. Bogaert, P.; Lamarche, C.; Defourny, P. Hidden Markov Models for Annual Land Cover Mapping—Increasing Temporal Consistency and Completeness. *IEEE Trans. Geosci. Remote Sens.* **2022**, *60*, 1–14. [CrossRef]
33. Ó Fionnagáin, D.; Geever, M.; O'Farrell, J.; Codyre, P.; Trearty, R.; Tessema, Y.; Reymondin, L.; Loboguerrero, A.M.; Spillane, C.; Golden, A. Assessing climate resilience in rice production: Measuring the impact of the Millennium Challenge Corporation's IWRM scheme in the Senegal River Valley using remote sensing and machine learning. *Environ. Res. Lett.* **2024**, *19*, 074075. [CrossRef]
34. Higginbottom, T.P.; Adhikari, R.; Foster, T. Rapid expansion of irrigated agriculture in the Senegal River Valley following the 2008 food price crisis. *Environ. Res. Lett.* **2023**, *18*, 014037. [CrossRef]

35. Abercrombie, S.; Friedl, M. Improving the Consistency of Multitemporal Land Cover Maps Using a Hidden Markov Model. *IEEE Trans. Geosci. Remote Sens.* **2015**, *54*, 1–11. [CrossRef]
36. Duke, N.; Burns, K. Fate and Effects of Oil and Dispersed Oil on Mangrove Ecosystems in Australia. 1999. Available online: https://www.researchgate.net/publication/37629636_Fate_and_Effects_of_oil_and_dispersed_oil_on_mangrove_ecosystems_in_Australia (accessed on 19 January 2025).
37. Orimoogunje, O.; Ajibola-James, O. Mangrove Ecosystem Recovery and Restoration from Oil Spill in the Niger Delta: The GIS Perspective. Geoinfor Geostat: An Overview S1. *Geoinform. Geostat. Overv.* **2013**, *5*, 2.
38. Getter, C.; Lewis, R. Spill Response that Benefits the Long-Term Recovery of Oiled Mangroves. *Int. Oil Spill Conf. Proc.* **2003**, *2003*, 539–550. [CrossRef]
39. M'rabu, E.; Bosire, J.O.; Cannicci, S.; Koedam, N.; Dahdouh-Guebas, F. Mangrove die-back due to massive sedimentation and its impact on associated biodiversity. *Kenya Aquat. J.* **2012**, *9*, 45–59.
40. Ohimain, E.I.; Andriesse, W.; van Mensvoort, M.E. Environmental impacts of abandoned dredged soils and sediments: Available options for their handling, restoration and rehabilitation. *J. Soils Sediments* **2004**, *4*, 59–65. [CrossRef]
41. Awosika, L.; Folorunsho, R. Estuarine and Ocean Circulation Dynamics in the Niger Delta, Nigeria: Implications for Oil Spill and Pollution Management. In *Environmental Management of Oil Spill in the Niger Delta*; Springer: Berlin/Heidelberg, Germany, 2014; pp. 77–86. ISBN 978-3-319-06387-4. [CrossRef]
42. Gordon, G.; Stavi, I.; Shavit, U.; Rosenzweig, R. Oil spill effects on soil hydrophobicity and related properties in a hyper-arid region. *Geoderma* **2018**, *312*, 114–120. [CrossRef]
43. Watts, M.; Zalik, A. Consistently unreliable: Oil spill data and transparency discourse. *Extr. Ind. Soc.* **2020**, *7*, 790–795. [CrossRef] [PubMed]
44. Ojiako J.C, Duru U.U, R. Use of Remote Sensing Data to Detect Environmental Degradation in the Oil Rich Region of Southern Nigeria between 2003 and 2015. *Int. J. Environ. Agric. Biotechnol.* **2017**, *2*, 2503–2508. [CrossRef]
45. Dutsenwai, H.S.; Ahmad, B.B.; Tanko, A.I.; Mijinyawa, A. Spatio-temporal analysis of vegetation and oil spill intensity in Ogoniland. *Int. J. Adv. Appl. Sci.* **2017**, *4*, 81–90. [CrossRef]
46. Farhana Ahmad, S.S.; Hazrina Idris, N. Oil Spill Impacts on Mangrove Forest from Satellite Remote Sensing. In Proceedings of the 2021 7th International Conference on Space Science and Communication (IconSpace), Selangor, Malaysia, 23–24 November 2021; pp. 60–64. [CrossRef]
47. Gundlach, E.R.; Bonte, M.; Story, N.I.; Iroakasi, O. Using high-resolution imagery from 2013 and 2020 to establish baseline vegetation in oil-damaged mangrove habitat prior to large-scale post-remediation planting in Bodo, Eastern Niger Delta, Nigeria. *Remote Sens. Appl. Soc. Environ.* **2022**, *28*, 100831. [CrossRef]
48. Lassalle, G.; Scafutto, R.D.M.; Lourenço, R.A.; Mazzafera, P.; de Souza Filho, C.R. Remote sensing reveals unprecedented sublethal impacts of a 40-year-old oil spill on mangroves. *Environ. Pollut.* **2023**, *331*, 121859. [CrossRef] [PubMed]
49. Bashir Adamu, K.T.; Ogutu, B. Using vegetation spectral indices to detect oil pollution in the Niger Delta. *Remote Sens. Lett.* **2015**, *6*, 145–154. [CrossRef]
50. Pavanelli, D.D.; Loch, C. Mangrove spectra changes induced by oil spills monitored by image differencing of normalised indices: Tools to assist delimitation of impacted areas. *Remote Sens. Appl. Soc. Environ.* **2018**, *12*, 78–88. [CrossRef]
51. Giri, C. Recent Advancement in Mangrove Forests Mapping and Monitoring of the World Using Earth Observation Satellite Data. *Remote Sens.* **2021**, *13*, 563. [CrossRef] [PubMed]
52. Nababa, I.I.; Symeonakis, E.; Koukoulas, S.; Higginbottom, T.P.; Cavan, G.; Marsden, S. Land Cover Dynamics and Mangrove Degradation in the Niger Delta Region. *Remote Sens.* **2020**, *12*, 3619. [CrossRef]
53. Ghorbanian, A.; Zaghian, S.; Asiyabi, R.M.; Amani, M.; Mohammadzadeh, A.; Jamali, S. Mangrove Ecosystem Mapping Using Sentinel-1 and Sentinel-2 Satellite Images and Random Forest Algorithm in Google Earth Engine. *Remote Sens.* **2021**, *13*, 2565. [CrossRef]
54. Upakankaew, K.; Ninsawat, S.; Virdis, S.G.P.; Sasaki, N. Discrimination of Mangrove Stages Using Multitemporal Sentinel-1 C-Band Backscatter and Sentinel-2 Data—A Case Study in Samut Songkhram Province, Thailand. *Forests* **2022**, *13*, 1433. [CrossRef]

Disclaimer/Publisher's Note: The statements, opinions and data contained in all publications are solely those of the individual author(s) and contributor(s) and not of MDPI and/or the editor(s). MDPI and/or the editor(s) disclaim responsibility for any injury to people or property resulting from any ideas, methods, instructions or products referred to in the content.